

Atmospheric gravity waves from the impact of comet Shoemaker-Levy 9 with Jupiter

A. P. Ingersoll and H. Kanamori

Division of Geological and Planetary Sciences, California Institute of Technology, Pasadena

T. E. Dowling

Department of Earth, Atmospheric, and Planetary Sciences, Massachusetts Institute of Technology, Cambridge

Abstract. We study the effect of the Jovian water cloud on internal gravity waves generated by the impact of comet SL9. Vertical structure follows Voyager data to the 1-bar level, a moist adiabat from 1 to 5 bars, and a dry adiabat below the 5-bar level. The waves are trapped in the moist layer and propagate horizontally. Their speed is related to the vertical integral of the Brunt-Väisälä frequency, and varies as the square root of the water abundance (130 m/s for solar composition). The amplitudes are large, e.g., ± 1 K at a distance of 8000 km for an energy of 10^{27} ergs. The circular ripples should be detectable one or two days after the impact in thermal infrared and visible images.

Introduction

At the "Comet Pre-Crash Bash" held in Tucson on August 23-24, 1993, Dowling proposed that internal gravity waves spreading out from the impact would provide important information about the vertical thermal structure of Jupiter's atmosphere at levels below those probed by Voyager and other remote sensing instruments. *Achterberg and Ingersoll* [1989] (henceforth AI89) had argued that moist convection in the water cloud produces a stable layer in the 3- to 5-bar pressure range that acts as a waveguide, allowing only horizontal propagation [see also *Flasar and Gierasch*, 1986; *Allison*, 1990]. The first mode of the waveguide propagates the fastest, and for a nominal water abundance its phase speed is 130 m/s. Dowling noted that waves from the impact measure the speed of this mode and hence the thermal structure of the water cloud.

Harrington et al. [1994] (henceforth H94) studied the impact-generated waves using a nonlinear, three-dimensional, primitive equation model. They found gravity waves with speeds up to 400 m/s in the stratosphere, but no selection of particular phase speeds and no amplitudes greater than 1.2 K for impact energies up to 10^{29} ergs. But with only five active layers in the vertical, they did not include the water cloud in their model and hence did not study the waveguide modes.

Copyright 1994 by the American Geophysical Union.

Paper number 94GL01057
0094-8534/94/94GL-01057\$03.00

Here we emphasize the waveguide effect of the water cloud. The model is linear and axisymmetric (i.e., two dimensional—radial and vertical), and follows chapters 6 and 7 of *Gill* [1982]. As in H94, the waves do not propagate into Jupiter's interior because it is assumed to be adiabatic. The basic state permits analytic solution of the the disturbance equations, so our model has continuous vertical structure. We model the upward propagation of energy without an artificial "sponge" by integrating over a continuous spectrum of vertical wavenumbers (*Gill*, section 6.12).

The hydrostatic approximation limits our analysis to low-frequency disturbances whose horizontal scale is much greater than the atmospheric scale height. It filters out the high-frequency compressional waves that propagate into Jupiter's interior at speeds of ~ 10 km/s [*Kanamori*, 1993; *Marley*, 1994; *Hunten et al.*, 1994]. The axisymmetric assumption limits our analysis to the area near the impact where the Coriolis parameter f can be considered constant. It entails neglecting the zonal wind variations with latitude, which are ± 20 m/s near the impact point. These approximations are valid during the first 1-2 days for wave speeds of 100-400 m/s.

Model

The basic equations and notation are *Gill's* (6.17.19) and (6.17.23), with a modification of the former to take into account rotation and cylindrical geometry:

$$\left(\frac{\partial^2}{\partial t^2} + f^2\right) \left(\frac{\partial w_*}{\partial z_*} - \frac{w_*}{H_*}\right) = \frac{1}{r} \frac{\partial}{\partial r} \left(r \frac{\partial^2 \Phi''}{\partial r \partial t}\right), \quad (1)$$

where H_* is a reference scale height. From *Gill* (6.17.25) it follows that $N_* H_* = NH$, where N is the Brunt-Väisälä frequency and H is the true scale height.

We separate variables as in *Gill* (6.17.34). The vertical basis functions $\hat{\Phi}$ and \hat{h}_* are the solutions of (6.17.35) and (6.17.36), with c_e the separation constant ($c_e^2/g = H_e =$ equivalent depth). The lower boundary condition (LBC) is $\hat{\Phi} = 0$ at the base of the water cloud (top of the adiabatic interior), where the pressure is P_* and z_* is zero [see *Gill* (6.17.8)]. This LBC has been shown to hold for quasi-geostrophic motions in a thin weather layer [*Gierasch et al.*, 1979; AI89]. Using the anelastic equations [*Ogura and Phillips*, 1962; *Ingersoll and Pollard*, 1982], but not the hydrostatic approxima-

tion, one can show that it holds also for gravity waves in a thin weather layer provided $k^2 H^2 \ll 1$, where k is the horizontal wavenumber of the disturbance.

Our model has $N_* H_* = c_0 = \text{constant}$ in the stratosphere, i.e., above the level where $P = P_0$ (Fig. 1). There the basis functions are sinusoids with argument mz_* . The vertical wavenumber m determines $c_e(m)$:

$$m^2 + \frac{1}{4H_*^2} = \frac{N_*^2}{c_e^2}. \quad (2)$$

Since $m^2 > 0$, it follows that $c_e < 2c_0$ (~ 900 m/s).

The complete solution is an integral over m from 0 to ∞ as in Gill (6.12.2), with $\rho_*^{1/2} \Phi''$ instead of h , and $\hat{\Phi}$ instead of $\sin(mz)$ [see also Gill (6.17.34)]. We normalize the basis functions by requiring that $\hat{\Phi}(mz_*)$ be a sinusoid of unit amplitude in the stratosphere ($0 \leq P \leq P_0$). Since the stratosphere extends to infinity in z_* , its contribution dominates that of the troposphere ($P_0 \leq P \leq P_r$) in integrals over z_* . Therefore we treat (6.12.2) as a Fourier sine transform and use the usual $2/\pi$ factor in taking its inverse. The same result is obtained using discrete Fourier series with a rigid lid at $z_* = L$, and then letting $L \rightarrow \infty$.

Our model has $N_* H_* = c_1 P/P_r$ in the troposphere (Fig. 1). Thus $\hat{\Phi}$ is proportional to $\rho_*^{1/2} \sin[c_1(P/P_r - 1)/c_e]$ for $P_0 \leq P \leq P_r$. Matching $\hat{\Phi}$ and \hat{h}_* at $P = P_0$, we obtain the normalized basis functions throughout the atmosphere ($0 \leq P \leq P_r$). We choose c_0 , c_1 , P_0 , and P_r by requiring that the mean temperature match the Voyager profile at 1 mbar, be continuous at $P = P_0$, and match the amplitude and height of the first peak in the response function in Fig. 3 of AI89.

Scaling arguments suggest that the momentum of the comet is negligible compared to the energy, as a source of gravity waves. The ratio of the two effects varies as c_e/v_c , where v_c is the velocity of the comet, about 60,000 m/s, and c_e is of order 130 m/s. Adopting a Green's function approach, we assume that the comet releases energy in a vertical line at $r = 0$. Allowing for the finite area of the source requires convolving our results with an appropriate horizontal weighting function.

The initial temperature perturbation is Q/C_p , where Q is the energy deposited per unit mass and C_p is the heat capacity. Gill's (6.17.23) gives the initial Φ'' :

$$\left. \frac{\partial \Phi''}{\partial z_*} \right|_{t=0} = \frac{\kappa Q}{H_*} = \frac{\kappa g}{H_*} q(z_*) \delta(r). \quad (3)$$

Here κ is the ratio R/C_p where R is the gas constant; $q(z_*)$ is the energy deposited per unit pressure interval; and $\delta(r)$ is a delta function defined so that the integral $2\pi \int \delta(r) r dr$ is unity. We choose a simple analytic form for $q(z_*)$, namely $q = q_0 = \text{constant}$ for $0 \leq P \leq P_0$, and $q = q_0 (P/P_0) \exp[-(P - P_0)/P_m]$ for $P_0 \leq P \leq P_r$. For $P_0 < P_m < P_r$, $q(z_*)$ has a maximum in the troposphere at $P = P_m$. Our nominal model has $P_m = \infty$. No energy is deposited at levels where $P > P_r$.

Combining Eqs. (1), (3), and Gill's (6.17.23) we obtain the equation for the steady part of the solution

$\Phi''(r, z_*)$ in terms of the forcing function $q(z_*)$:

$$\frac{1}{r} \frac{\partial}{\partial r} \left(r \frac{\partial \Phi''}{\partial r} \right) + \frac{f^2}{\rho_*} \frac{\partial}{\partial z_*} \left[\frac{\rho_*}{N_*^2} \left(\frac{\partial \Phi''}{\partial z_*} - \frac{\kappa g q \delta}{H_*} \right) \right] = 0. \quad (4)$$

This equation, which is analogous to Gill's (7.2.20), follows from the conservation of potential vorticity. The second-order operator in z_* is the same as \mathcal{L} in AI89. The eigenvalue λ of this operator is the same as f/c_e .

Multiplying Eq. (4) by $\rho_*^{1/2} \hat{\Phi}$ and integrating over z_* from 0 to ∞ , we obtain an ordinary differential equation for $\tilde{\eta}_s(r; m)$ [see Gill (6.17.34)]. The solution involves the modified Bessel function $K_0(fr/c_e)$. Integrating over m , the steady part of the solution is

$$\Phi''(r, z_*) = \frac{f^2}{2\pi} \int_0^\infty \rho_*^{-1/2} \hat{\Phi}(z_*) D(m) K_0\left(\frac{fr}{c_e}\right) dm, \quad (5)$$

$$D(m) = \frac{2}{\pi} \int_0^\infty \rho_*^{-1/2} \hat{\Phi}(z_*) \frac{\partial}{\partial z_*} \left(\frac{\rho_* \kappa g q}{N_*^2 H_*} \right) dz_*. \quad (6)$$

The integral in (6) is done analytically. The $2/\pi$ factor comes from the Fourier sine transform.

The transient solution follows as in section 7.3 of Gill, which is for a single layer and Cartesian geometry. We have continuous vertical structure and cylindrical geometry, so the separation constant $c_e(m)$ replaces c and the Bessel function $J_0(kr)$ replaces $\sin(kx)$. Key integrals are (8.13.2) and (8.2.41) of Erdélyi [1954]. The Green's function analogous to Gill's (7.3.14) is, for $t > r/c_e$,

$$G(r, t; m) = \frac{1}{2\pi c_e^2} \frac{\cos \left[f \left(t^2 - r^2/c_e^2 \right)^{1/2} \right]}{\left(t^2 - r^2/c_e^2 \right)^{1/2}}, \quad (7)$$

with $G(r, t; m) = 0$ otherwise. The normalization is such that $\partial G/\partial t$ is equal to $\delta(r)$ at $t = 0$.

The complete solution for $\Phi''(r, z_*, t)$ is

$$\Phi''(r, z_*, t) = \frac{\partial \Psi}{\partial t}(r, z_*, t) + f^2 \int_0^t \Psi(r, z_*, t') dt', \quad (8)$$

$$\Psi(r, z_*, t) = \int_0^\infty \rho_*^{-1/2} \hat{\Phi}(z_*) c_e^2 D(m) G(r, t; m) dm. \quad (9)$$

The first term in (8) satisfies the initial condition (3) and tends to zero at large t . The second term is initially zero and tends to the steady solution (5) at large t .

The integrations in (5), (8), and (9), and the differentiation in (8) are performed numerically. The square-root singularity in G , although integrable, produces noise in the expression for Ψ . The noise is amplified on taking the time derivative, but is suppressed by filtering and by going to a finer step size in m .

Results

Figure 1 shows our nominal $N(P)$ profile compared to that in Fig. 2 of AI89. The latter uses Voyager data and a moist adiabat with solar water abundance. Our

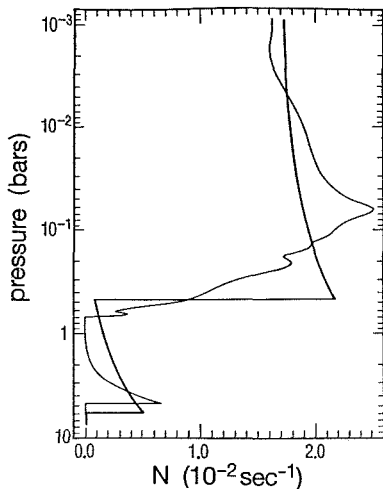


Figure 1. Brunt-Väisälä frequency N versus pressure for the nominal basic state. The thin wiggly line is the Voyager radio occultation profile with a moist adiabat below the 0.7-bar level [after *Achterberg and Ingersoll, 1989*]. The heavy smooth line is the nominal model with $c_0 = 447$ m/s, $c_1 = 222$ m/s, $P_0 = 0.472$ bar, and $P_r = 5.44$ bar.

profile mimics the response function shown in Fig. 3 of AI89. Two parameters match exactly—the location of the first resonance and its peak-to-trough ratio. The former determines the speed of the wave, and the latter determines the leakiness of the waveguide and hence the amplitude in the stratosphere. Leakiness is determined more by the thickness of the low- N region (~ 0.5 to 2 bar) than by the value of N there.

Resonances in the waveguide produce peaks in $D(m)$ similar to those in Fig. 3 of AI89. Each peak corresponds to a distinct mode of the waveguide—the first mode spanning one quarter-cycle in the troposphere, the next mode three quarter-cycles, and so on. The stratospheric wavenumber mH_s , in units of inverse scale heights, is 3.4 for the first mode and 16.4 for the second. The basis functions $\rho_*^{-1/2} \hat{\Phi}$ of the first two resonant modes resemble those plotted in Fig. 4 of AI89.

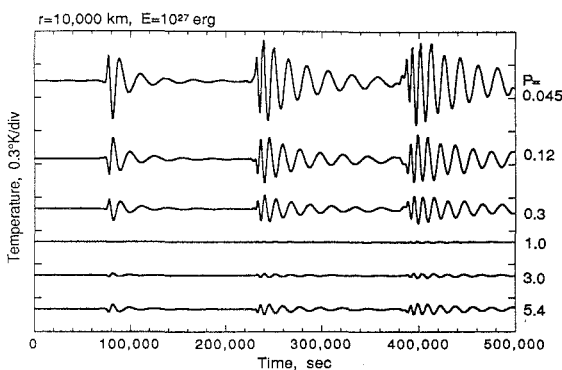


Figure 2. Temperature versus time at a fixed radial distance 10,000 km from the impact point for six different pressures (given in bars on the right side). Total energy is 10^{27} erg. The heating per unit pressure interval is constant in the stratosphere and is proportional to pressure in the troposphere ($P_m = \infty$).

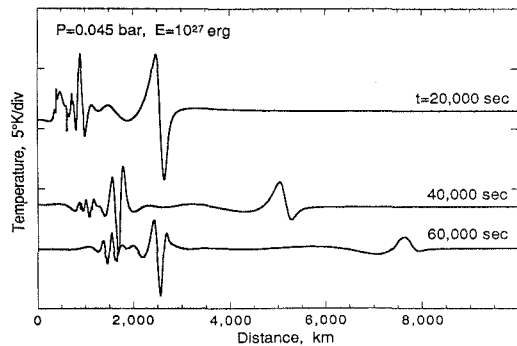


Figure 3. Temperature versus radius at three fixed times after the impact. The energy is 10^{27} erg, and the pressure is 0.045 bar. The heating profile is the same as in Fig. 2.

There are no discrete modes—modes with negative m^2 that decay with height in the stratosphere.

The values of mH_s for our nominal model are somewhat larger than the values $2\pi/3 = 2.1$ and $2\pi/0.5 = 12.6$ inferred by *Allison [1990]* from vertical variations in the Voyager radio occultation profiles. Allison interprets these variations as waves leaking out of the tropospheric waveguide, and infers a water abundance there that is 2 or 3 times the solar value. The inference is qualitatively consistent with (2), since smaller m implies larger c_e and hence larger values of NH . From the observed maximum speed of westward-propagating waves, *Williams and Yamagata [1984]* infer an upper bound $c_e = \sqrt{gH_e} \leq 155$ m/s (see their discussion of the L_R scale on p. 459), in good agreement with the estimates of AI89 and Allison.

Resonant modes dominate the response to the impact. Even in the stratosphere the disturbance is a series of separate pulses, each travelling at the speed c_e of a tropospheric mode. Figure 2 shows the time series of temperature at a point 10,000 km from the impact, for six different pressure levels in the atmosphere. From left to right, the three pulses are the first, second, and third modes of the waveguide. As shown in section 7.3 of Gill, the short horizontal wavelengths are non-dispersive and have the largest group velocity, which in this case is c_e . The short waves from the first mode are the fastest, and have a speed of 130 m/s for this nominal model. According to AI89, the speed varies as the square root of the water abundance. For each mode, the longer waves propagate away more slowly, eventually leaving only the waves with zero group velocity—inertial oscillations with frequency f . The detailed shape of each pulse varies with altitude because the resonant modes oscillate with respect to z_* (Fig. 4 of AI89).

Figure 3 shows profiles of temperature versus radius at three different times after the impact, for a pressure level of 0.045 bar. The pulse farthest from the origin is the first mode. In an infrared image tuned to this pressure level, the disturbance would appear as three concentric rings representing the first three tropospheric modes. The amplitude of each pulse decreases as $1/r^2$ because both the radial width and the circumference of

the disturbed fluid vary as r . Up to a point, the disturbance amplitude is proportional to the initial energy and inversely proportional to c_1^2 , which is $N^2 H^2$ for the tropospheric waveguide. This dependence holds until the amplitude gets too large and the waveguide gets too weak (small c_1^2), at which point the scaling breaks down. These curves (Figs. 2 and 3) are for $P_m = \infty$, meaning that the heating per unit pressure interval q is constant in the stratosphere and is proportional to pressure in the troposphere. For smaller values of P_m the heating is concentrated at higher altitudes, and the amplitude of the first mode is smaller.

The disturbance amplitude is large, especially at the higher altitudes. At 8000 km from the source (Fig. 3), the amplitude of the temperature perturbation is ± 1 K at $P = 0.045$ bar. The associated vertical velocity is ± 5 m/s. These numbers are for an impact energy of 10^{27} ergs, which is a modest-sized fragment, 0.5 km in diameter, if it were made of solid ice. The amplitudes are not totally realistic, however, because the wave would break close to the source, causing the heated fluid to mix. Such mixing is treated in our linear model by spreading the initial energy over a finite area. For a disk of radius 200 km and energy 10^{27} ergs, we find that the tropospheric amplitudes never exceed 25 K, which is only 10% of T itself and therefore within the range of linear theory. This amount of spreading has little effect on the amplitudes at $r = 8000$ km. The stratospheric waves will probably break close to the source but will reappear downstream as in Figs. 2 and 3 after leaking up from the tropospheric waveguide. Impacts of order 10^{29} ergs will excite detectable stratospheric waves that are not tied to the tropospheric waveguide (H94). These waves propagate at speeds up to 400 m/s, but they have smaller amplitudes than those studied here and will be unobservable for the smaller impacts.

The encouraging result from this linear theory is that gravity waves should be visible even for relatively small impacts. If the disturbance rings can be seen, regardless of conditions near the source, then we will have an estimate of the thermal structure in the water cloud and an estimate of the Jovian water abundance.

Acknowledgments. Dowling and Ingersoll acknowledge support from NASA's Planetary Atmospheres Pro-

gram, grants NAGW-2956 and NAGW-1956; Kanamori acknowledges support from NSF grant EAR-92 18809.

References

- Achterberg, R.K., and A.P. Ingersoll, A normal-mode approach to Jovian atmospheric dynamics, *J. Atmos. Sci.*, **46**, 2448, 1989.
- Allison, M., Planetary waves in Jupiter's equatorial atmosphere, *Icarus*, **83**, 282, 1990.
- Erdélyi, A., ed., *Tables of Integral Transforms, Volume 2*, McGraw-Hill, New York, 1954.
- Flasar, F.M., and P.J. Gierasch, Mesoscale waves as a probe of Jupiter's deep atmosphere, *J. Atmos. Sci.*, **43**, 2683, 1986.
- Gierasch, P.J., A.P. Ingersoll, and D. Pollard, Baroclinic instabilities in Jupiter's zonal flow, *Icarus*, **40**, 205, 1979.
- Gill, A.E., *Atmosphere-Ocean Dynamics*, Academic Press, San Diego, 1982.
- Harrington, J., R.P. LeBeau, K.A. Backes, and T.E. Dowling, Dynamic response of Jupiter's atmosphere to the impact of comet Shoemaker-Levy 9, *Nature*, **368**, 525, 1994.
- Hunten, D.M., W.F. Hoffmann, and A.L. Sprague, Jovian seismic waves and their detection, *Geophys. Res. Lett.*, in press, 1994.
- Ingersoll, A.P., and D. Pollard, Motion in the interiors and atmospheres of Jupiter and Saturn: Scale analysis, anelastic equations, barotropic stability criterion, *Icarus*, **52**, 62, 1982.
- Kanamori, H., Excitation of Jovian normal modes by an impact source, *Geophys. Res. Lett.*, **20**, 2921, 1993.
- Marley, M., Seismological consequences of the collision of comet Shoemaker-Levy/9 with Jupiter, *Astrophys. J. Lett.*, in press, 1994.
- Ogura, Y., and N.A. Phillips, Scale analysis of deep and shallow convection in the atmosphere, *J. Atmos. Sci.*, **19**, 173, 1962.
- Williams, G.P., and T. Yamagata, Geostrophic regimes, intermediate solitary vortices and Jovian eddies, *J. Atmos. Sci.*, **41**, 453, 1984.

T. E. Dowling, Department of Earth, Atmospheric, and Planetary Sciences, MIT, Cambridge, MA 02139.

A. P. Ingersoll and H. Kanamori, Division of Geological and Planetary Sciences, Caltech, Pasadena, CA 91125.

(received March 4, 1994; revised April 11, 1994; accepted April 14, 1994.)